



Nematic superconductivity in LiFeAs

Y. S. Kushnirenko ¹, D. V. Evtushinsky,^{1,2} T. K. Kim,³ I. Morozov,^{1,4} L. Harnagea ^{1,5}, S. Wurmehl,¹
S. Aswartham,¹ B. Büchner,^{1,6} A. V. Chubukov,⁷ and S. V. Borisenko¹

¹*IFW Dresden, Helmholtzstrasse 20, 01069 Dresden, Germany*

²*Institute of Physics, Ecole Polytechnique Federale Lausanne, 1015 Lausanne, Switzerland*

³*Diamond Light Source, Harwell Campus, Didcot OX11 0DE, United Kingdom*

⁴*Department of Chemistry, Lomonosov Moscow State University, 119991 Moscow, Russia*

⁵*Indian Institute of Science Education and Research, Pune, Maharashtra 411008, India*

⁶*Institute for Solid State and Materials Physics, TU Dresden, 01062 Dresden, Germany*

⁷*Department of Physics, University of Minnesota Twin Cities, Minneapolis, Minnesota 55455, USA*



(Received 7 April 2020; revised 22 June 2020; accepted 12 October 2020; published 3 November 2020)

The role of nematic order for the mechanism of high-temperature superconductivity is highly debated. In most iron-based superconductors (IBSs) the tetragonal symmetry is broken already in the normal state, resulting in orthorhombic lattice distortions, static stripe magnetic order, or both. Superconductivity then emerges, at least at weak doping, already from the state with broken C_4 rotational symmetry. One of the few stoichiometric IBSs, lithium iron arsenide superconducts below 18 K and does not display either structural or magnetic transition in the normal state. Here we demonstrate, using angle-resolved photoemission spectroscopy, that even the superconducting state in LiFeAs is also a nematic one. We observe spontaneous breaking of the rotational symmetry in the gap amplitude on all Fermi surfaces, as well as unidirectional distortion of the Fermi pockets. Remarkably, these deformations are hardly visible above superconducting T_c . Our results demonstrate the realization of the phenomenon of superconductivity-induced nematicity in IBSs, emphasizing the intimate relation between them. We suggest a theoretical explanation based on the emergence of a secondary instability inside the superconducting state, which leads to the nematic order and s - d mixing in the gap function.

DOI: [10.1103/PhysRevB.102.184502](https://doi.org/10.1103/PhysRevB.102.184502)

I. INTRODUCTION

Several classes of materials which become superconducting at elevated temperatures also show a spontaneous unidirectional order in some part of their phase diagrams. Examples range from stripes, directly observed in the cuprates [1] and in FeSe films [2], to the nematic liquid state in the ruthenates [3] and to the rotational symmetry breaking state in iron-based superconductors (IBSs) [4]. Nematicity has been one of the central topics in studies of IBSs for the last decade [5,6]. It leads to significant anisotropy of the magnetic properties [7] and of the electronic transport [4], orthorhombic distortions of the lattice [8–11], and sizable changes in the low-energy electron dynamics, e.g., band splitting close to the Fermi level, which in FeSe well exceeds the superconducting gap [12,13]. Raman and other data [14–20] on several IBSs reveal a strong increase of the nematic susceptibility, which starts well above the nematic transition temperature. The issue, which received less attention until recently, is the relation between nematicity and superconductivity. From the theory perspective, nematic fluctuations can mediate superconductivity [21,22], and long-range nematic order affects both the gap structure and superconducting T_c , as recent studies of FeSe_{1-x}S_x have demonstrated [23]. In this work we discuss whether superconductivity can, in turn, induce or enhance a nematic order. This issue attracted a lot of attention recently

with the discovery of nematic superconductivity in the doped topological insulator Bi₂Se₃ [24–28] and in twisted bilayer graphene [29–34].

In this paper we report the observation of nematic superconductivity in stoichiometric lithium iron arsenide (LiFeAs). It is tetragonal in the normal state and shows no magnetic or structural transition before it becomes superconducting at $T_c = 18$ K [35]. Earlier data in the superconducting state were interpreted assuming that C_4 symmetry remains intact. It was shown recently that application of strain induces rotational symmetry breaking in the superconducting state of LiFeAs [36]. We show here that in the superconducting state LiFeAs actually develops a spontaneous nematic order.

II. MATERIALS AND METHODS

LiFeAs single crystals in the form of packets of plates with dimensions of up to 1 cm were grown by self-flux using the standard method [37]. For the angle-resolved photoemission spectroscopy (ARPES) study single-crystal plates with dimensions of $3 \times 3 \times 0.1 \text{ mm}^3$ were selected. The single crystals were prepared for measurements in a dry argon box. Experiments were carried out at the I05 beamline of the Diamond Light Source [38]. Single-crystal samples were cleaved *in situ* in a vacuum better than 2×10^{-10} mbar. Measurements were performed using linearly polarized

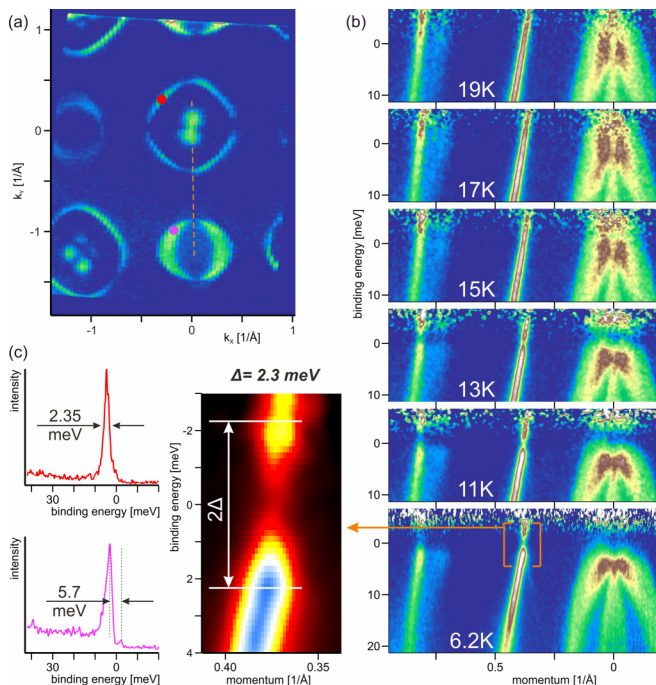


FIG. 1. Superconducting gaps from ARPES. (a) Overview Fermi surface map taken using 80-eV photons. (b) Intensity plots corresponding to the dashed line in (a) measured as a function of temperature with 21-eV photons. All spectra are divided by the Fermi function to enhance the signal above the Fermi level. (c) Exemplary EDCs from the k points marked in (a) by red and magenta dots. The 2D intensity plot corresponds to the area limited by the square brackets in the bottom panel of (b).

synchrotron light with photon energies in a range from 18 to 80 eV, utilizing a Scienta R4000 hemispherical electron energy analyzer with an angular resolution of 0.2° – 0.5° and an energy resolution of 2–5 meV. None of the maps presented in the paper are symmetrized.

III. RESULTS

In order to study possible signs of nematicity in superconducting LiFeAs we revisit its electronic structure and, especially, the gap function, using angle-resolved photoemission spectroscopy with a new level of precision.

In Fig. 1(a) we show a Fermi surface (FS) map which roughly covers the single iron atom (1-Fe) Brillouin zone, often used in theoretical studies. This map represents all the main features of the electronic structure of LiFeAs. The “dumbbell” in the center and the corresponding four-point feature in the corner at approximately $(-1.2, -1.2)$ are associated with the small d_{xz}/d_{yz} holelike pocket. The large square with rounded corners, also centered at the Γ point, is the d_{xy} holelike Fermi surface, and the pockets centered at approximately $(-1.2, 0)$ and $(0, -1.2)$ are electronlike Fermi surfaces, formed by the d_{xy} orbital and either the d_{xz} or d_{yz} orbital. We will refer to the coordinate system of Fig. 1(a) throughout the paper. Panels in Fig. 1(b) show the temperature evolution of the characteristic high-symmetry cut, indicated on the map [Fig. 1(a)] by the dashed orange line, which runs through all four Fermi surface sheets. From left to right, the dispersions correspond to d_{xy} , inner electron pocket; d_{yz} ,

outer electron pocket; d_{xy} , large hole pocket; d_{xz} , small hole pocket; and d_{yz} , dispersion, which does not cross the Fermi level. Each of the two latter dispersions changes its orbital character between d_{xz} and d_{yz} under a rotation in the XY plane but has a particular orbital character (d_{xz} or d_{yz}) along high-symmetry directions. Therefore, we label these dispersions and corresponding FS pockets d_{xz} or d_{yz} . As expected, the gap opens up at 17 K and gradually wipes out the spectral weight from the Fermi level as the temperature is lowered. It is seen from the presented data that the largest superconducting gap is on the small holelike pocket. It is about 5.4 meV at this particular k_z , as measured by fitting the corresponding energy-distribution curve. The next highest in magnitude is the gap on the inner electron pocket (~ 3.6 meV), and the smallest one is on the large d_{xy} Fermi pocket (~ 2.3 meV). Because this large hole pocket shows up in ARPES as a single dispersion, well separated from other dispersing features, the characteristic bending back of the dispersion is clearly seen in the bottom panel of Fig. 1(b). To underline the precision of our measurements, we zoom in on this minimal gap and show the result in Fig. 1(c) together with two typical energy-distribution curves (EDCs) from the k points marked on the map by red and magenta circles. Not only the sharpness of the EDCs but also the presence of the coherence peaks above the Fermi level [Figs. 1(b) and 1(c)] demonstrates that the superconducting gap in LiFeAs can be measured by ARPES with very high precision (for details of the gap extraction from the data see Appendix A).

First, we consider in detail the features associated with the hole pockets at the center of the Brillouin zone (BZ). The high-resolution data set, shown in Fig. 2(a), is recorded under special geometry conditions to minimize the influence of the matrix element effects ($h\nu = 25$ eV). If one compares the maps from Figs. 1(a) and 2(a), one can immediately notice that the pronounced minima along k_x and k_y in the former are absent in the latter. This is achieved by rotating the sample by 22.5° . In this geometry the d_{xy} states are not strongly suppressed along any direction in the k space, providing a suitable nonsymmetrized data set for the gap extraction from the EDC line shape. The intensity in the map is still slightly asymmetric, but this has no influence on the line shape of the EDC. The gaps extracted from leading edges of such EDCs are plotted in Fig. 2(c) as functions of the angle along the Fermi surfaces (for details see Ref. [39]).

One of the central results of the present paper is immediately seen from Fig. 2(c): the gap function does not obey C_4 symmetry and has only two maxima and two minima, indicating C_2 rotational symmetry. We emphasize that the amplitude of the gap oscillations is considerable, well above the error bars. The gap modulation cannot be described by a single $\cos 2\theta$ function, indicating the presence of higher harmonics, including the $\cos 4\theta$ one. Another observation, overlooked in the earlier studies, is the deformation of the Fermi surface itself. In Fig. 2(b) we show the intensity distributions along k_x and k_y cuts [where k_x and k_y correspond to the coordinate system introduced in Fig. 1(a)]. Momentum distribution curves from the Fermi level (E_F -MDCs) clearly indicate that the large holelike Fermi surface is elongated in the k_y direction. Moreover, this conclusion is supported not only by the MDCs from the Fermi level. In Fig. 2(d) we plot the position of the maxima of MDCs as a function of

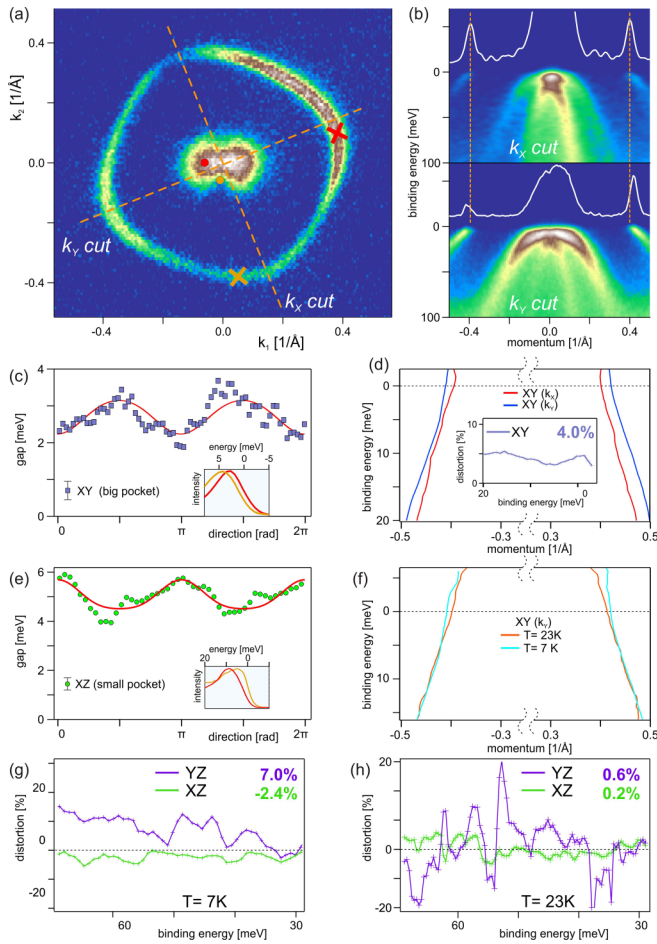


FIG. 2. Gap anisotropy and distortions of the holelike FS pockets and dispersions. (a) High-resolution FS map measured at 7 K with 25-eV photons, which approximately corresponds to $k_z = 0$. (b) Intensity distributions along the k_x and k_y cuts. White curves are E_F -MDCs. Vertical dashed lines help to compare the peak positions. (c) Gap function of the large hole pocket. Here the angle is counted counterclockwise from the k_y direction. Fitting function is mostly $\cos 2\theta$ with a small ($\sim 6\%$) admixture of higher harmonics. (d) Dispersions corresponding to the large hole pocket extracted from (b). The inset shows the behavior of the distortion coefficient. (e) Gap function of the small hole pocket. (f) Temperature dependence of the dispersions corresponding to the k_y cut. (g) Distortion coefficient for the xz and yz dispersions in the center of the BZ. (h) The same as (g), but measured at 23 K. Insets show EDCs from k points indicated by crosses and dots on the map in the energy scale with zero at the minimal leading-edge position. The error bars in the corners of (c) and (e) indicate standard error.

the binding energy. The plot demonstrates that the distortion persists to higher binding energies. We define a deformation coefficient as $D = 2 \frac{L_y - L_x}{L_y + L_x}$, where L_y and L_x are the pocket sizes ($2k_F$) in the X and Y directions, respectively. Its average value for the binding energy interval shown in the inset is 4%. The systematic error of the deformation coefficient is $\pm 1\%$ (for details see Ref. [39]). This systematic error can be caused by uncertainty in angle calibration of the electron analyzer and the manipulator. The random error in the data for a given energy is almost completely eliminated by averaging the deformation coefficient over an energy window.

In Figs. 2(e) and 2(g) we show the results for the two d_{xz}/d_{yz} hole dispersions near Γ . The results are similar to the ones for the d_{xy} pocket, but there are important differences. Strictly speaking, neither of the d_{xz}/d_{yz} dispersions crosses the Fermi level at this k_z , which is near the Γ point. Still, one of the dispersions comes close enough to the Fermi level and thus “feels” the gap. These bands are not degenerate in the center of the BZ because of the spin-orbit coupling [40,41], and one is able to consider the gap only on the d_{xz} component. The gap function extracted from the change in this dispersion below T_c is in antiphase with the one for the d_{xy} Fermi pocket [Fig. 2(e)], and it also has a clear C_2 symmetry rather than C_4 . Since the tops of both d_{xz}/d_{yz} dispersions are close to the Fermi level, the extraction of the distortions from the MDC dispersion near the Fermi level is quite complicated, and we have estimated the distortions by analyzing them at higher binding energies [Fig. 2(g)]. The distortions of the two d_{xz}/d_{yz} dispersions turned out to be of opposite sign and reached $7.0 \pm 1.0\%$ and $-2.4 \pm 1.0\%$. For the d_{yz} dispersion, the distance between its left and right branches is smaller, and their widths are larger. This results in the larger error bars of the distortion because the sum of two such distances is in the denominator. Nevertheless, averaging over the energy clearly signals the presence of the effect (see Figs. S3 and S4 in the Supplemental Material [39]).

Where do the observed distortions come from? Figure 2(f) demonstrates the temperature evolution of the dispersion upon crossing T_c . The evolution is highly atypical for a superconductor. Usually [42,43], the dispersion in the superconducting state develops a distinctive bending at higher binding energies and then runs vertically within the gap region and hits the Fermi level exactly at k_F , representing the so-called S-shaped dispersion. The data in Fig. 2(f), taken along k_y , show no S shape, but a momentum distance between branches of the dispersion grows in this particular direction. The results obtained from another sample (see Fig. 7 in Appendix C) also demonstrate such a behavior. The deformation is absent in the data taken above T_c [see Fig. 2(h)], or at least, it is significantly smaller. Moreover, the distortion of the d_{xy} dispersion also nearly disappears in the normal state (see Fig. 7 in Appendix C). This implies that the deformation is enhanced by superconductivity. In addition to the reasons mentioned above, the error bars for the d_{yz} distortion are large also because of the higher temperature, which additionally broadens the MDCs.

To have a complete overview of the rotational symmetry breaking in LiFeAs, we extended our high-resolution measurements to electronlike pockets. We show in Fig. 3(a) the FS map, taken using 25-eV photons, which corresponds to k_z 's closer to the ΓMX plane of the BZ (see Appendix B). As found earlier [40], because of the spin-orbit interaction, the electron pockets hybridize along the BZ boundaries and therefore should be described as inner and outer pockets rather than as crossed ellipses. For all k_z values, the inner pocket in LiFeAs is of d_{xy} character, and the outer one is of $d_{xz,yz}$ character. This is because the crossing of the bands, coming from the bottoms of electron pockets, is below E_F in the ΓMX plane [40]. In spite of the increased k_z resolution, the outer electron pocket in LiFeAs still appears blurred on the maps, where the k_z dispersion is strong. Because of this,

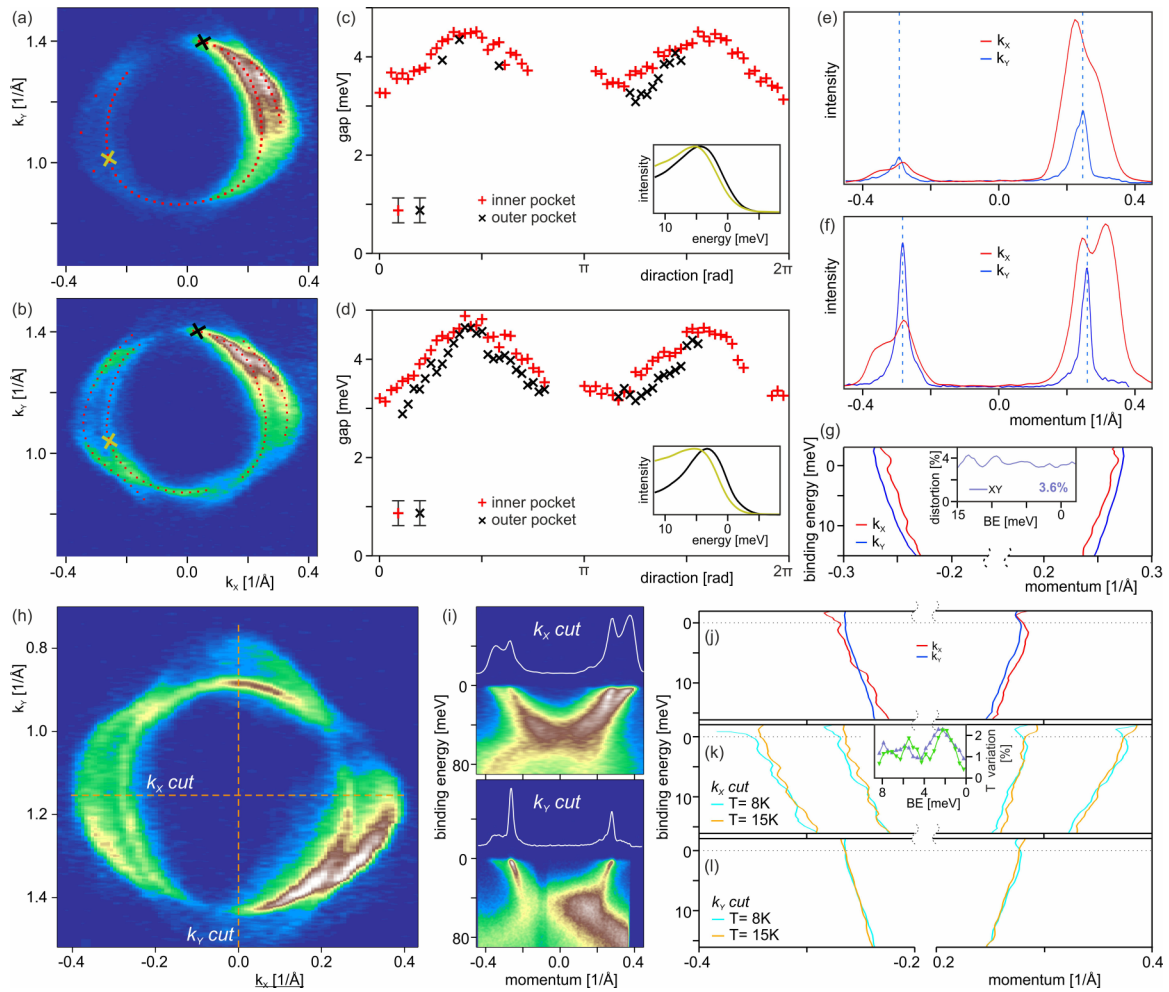


FIG. 3. Gap anisotropy and distortions of the electronlike FS pockets. (a) and (b) FS map of electron pockets measured with 25 eV ($k_z \sim 0$) and 23 eV photons, respectively. (c) and (d) Gap functions corresponding to (a) and (b). Here angle is counted counterclockwise from the k_y direction. Insets show EDCs from the points on the maps marked by the crosses of the same color in the energy scale with zero at the minimal leading-edge position. (e) and (f) E_F -MDCs corresponding to (a) and (b). Dashed lines indicate the different positions of the peaks. (g) Dispersions supporting the inner electron pocket from (b). The inset shows the distortion coefficient and its average value. (h) FS map at 21 eV, which roughly corresponds to $k_z = \pi$. (i) Intensity distribution along k_x and k_z cuts from (h) together with the corresponding E_F -MDCs. (j) Dispersions corresponding to the inner electron pocket from (h). (k) Temperature dependence of the dispersions along the k_x cut. The inset shows the temperature-induced size variation of the inner (green markers) and outer (purple markers) electron pockets, similar to the distortion coefficient. (l) Temperature dependence of the dispersions of the inner pocket along the k_y cut. No matching of the zero position has been done in (j)–(l). The error bars in the corners of (c) and (d) indicate standard error.

the gap function, shown in Fig. 3(c), contains more data points for the inner pocket than for the outer one. Nevertheless, both gaps are again twofold symmetric with strong modulation amplitude. The degree of the gap variations is easy to see directly from the EDCs in the inset. These EDCs are taken from the two k points marked by the small crosses. Again, the E_F -MDCs [Fig. 3(e)] show that the inner pocket is deformed and is longer along k_y . To analyze the outer electron pocket, we used incident photon energies $h\nu = 23$ and 21 eV. At $h\nu = 23$ eV the outer electron pocket is larger and more distinguishable from the inner one [Fig. 3(b)]. Figure 3(d) clearly shows that the gap on this pocket is twofold symmetric. The E_F -MDCs [Fig. 3(f)] show that the inner pocket is again elongated. Underlying dispersions [Fig. 3(g)] yield the average distortion coefficient $D = 3.6\% \pm 1.0\%$.

At $h\nu = 21$ eV the outer pocket is even larger and better separated from the inner one [Fig. 3(h)]. Two cuts along k_x and k_y show the underlying dispersions [Fig. 3(i)], and it is seen that, at least for the k_x cut, the dispersion features corresponding to the outer FS are much better defined. Figures 3(k) and 3(l) show the temperature dependence of the dispersions, and one can now see that the size of the outer pocket along k_x becomes noticeably larger upon entering the superconducting state. Almost no change occurs between above and below T_c along the k_y direction. Interestingly, the distortion of the inner d_{xy} pocket is now different [Fig. 3(j)]—the distortion coefficient D becomes negative.

Comparing the data from Figs. 3(k) and 3(l) with the ones presented in Fig. 2(f), one can see the drastically different temperature evolution of the dispersion at different places in the k space. Superconductivity can bend it forward or back

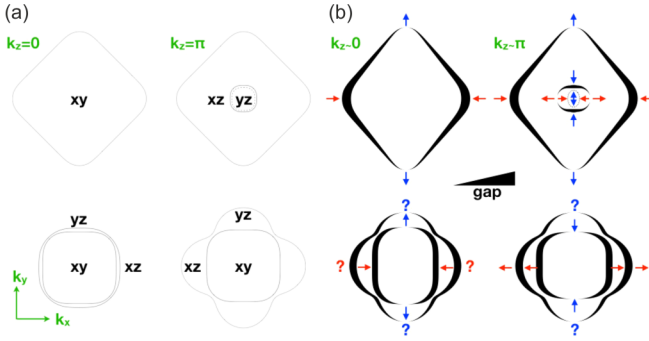


FIG. 4. (a) Schematic Fermi surface contours of LiFeAs from the experiments in the normal state. The dashed contour represents the yz states which do not cross the Fermi level. (b) Qualitative sketch of the distortions and gap anisotropies consistent with the experimental data. Red (blue) arrows indicate squeezing (stretching) of the FSs. Question marks indicate uncertainty in regard to the distortion of the outer electron pocket.

or leave it practically untouched. Remarkably, the dispersion bending [44] is most pronounced where the gap is the largest.

We summarize our experimental observations in Fig. 4, where we show all gap anisotropies and FS distortions. A sketch of the Fermi surface of LiFeAs in the normal state is given in Fig. 4(a) together with the orbital composition of the pockets. There is no small d_{xz}/d_{yz} pocket at Γ because d_{xz}/d_{yz} hole dispersions only approach the Fermi level without crossing it. The inner (outer) electron pockets are formed by d_{xy} (d_{xz}, d_{yz}) orbitals at all k_z 's. In Fig. 4(b) the observed gap variations are shown as the thickness of the Fermi contours. The minimal thickness corresponds to the minimal gap. Distortions are shown schematically, qualitatively reproducing the behavior of the deformation D . When the pocket size along k_y is larger, D is positive; when it is larger along k_x , D is negative. Question marks indicate that the distortion of the outer electron pocket is somewhat difficult to determine because of the broadening caused by strong k_z dispersion. Different signs of the distortion of the electron pockets at $k_z = 0$ and $k_z = \pi$ [different directions of arrows in Fig. 4(b)] may be due to the existence of the additional in-plane interaction channel at $k_z = \pi$ because at this k_z hole d_{xz}/d_{yz} dispersions cross the Fermi level. While the detailed k_z dependence of the observed effects still needs to be refined, calling for further, even more thorough experimental studies, Fig. 4 provides an overview of spontaneous rotational symmetry breaking in the superconducting state of LiFeAs.

IV. DISCUSSION

We now present a theoretical analysis of the observed variation of the gap on hole and electron pockets. The experimental facts most relevant to the analysis below are (i) the absence of the gap nodes on the d_{xy} hole pocket and (ii) the $\cos 2\theta$ variation of the gap along this pocket. The first observation implies that the gap is not a pure d wave; the second indicates that a d -wave gap component is present along with an s -wave component, i.e., $\Delta_{xy}(\theta) = \Delta_s + \Delta_d \cos 2\theta$. Such behavior is, indeed, expected when the system has a nematic order. Indeed, once C_4 symmetry is broken, s -wave and d -wave gap components are no longer orthogonal, and

the Landau free energy in general contains the symmetry-allowed term $\Delta_s \Delta_d$, linear in both s -wave and d -wave gap components. Because of bilinear coupling, once one pairing component develops, it acts as a field for the other component, and as a result, both are present.

The gap structure in LiFeAs was analyzed in several papers [45–48]. Like we said, the electronic structure of this material is somewhat different from those of other Fe pnictides in that cylindrical pockets in LiFeAs, which exist for all k_z values, are the two electron pockets and the d_{xy} hole pocket, centered at $k_x = k_y = \pm\pi$ in 1-Fe Brillouin zone, while d_{xz}/d_{yz} hole pockets, centered at $k_x = k_y = 0$, exist only around $k_z = \pi$. This electronic structure allows a competition between a number of possible pairing states, ranging from a conventional s^{+-} with a sign change between all hole and all electron pockets to orbitally antiphase s^{+-} with a sign change between d_{xz}/d_{yz} and d_{xy} hole pockets (and an additional sign change for the gap on a hole pocket and a portion of an electron pocket with the same orbital content) to several d -wave gap structures. Previous ARPES experiments were fitted better by an s -wave gap (the best fit is for the type A s^{+-} state in Ref. [45]), and we assume that in the absence of nematicity the gap would be an s wave. ARPES data reported here show that at $T = 23$ K, slightly above $T_c = 18$ K, the orthorhombic distortions are hard to detect, while the data taken at 7 K inside the superconducting state show nematic order. Assuming that the tetragonal symmetry is not broken above T_c , we are left with two options: it gets broken either at T_c or at some $T < T_c$. In both cases, s -wave superconductivity triggers C_4 symmetry breaking and the appearance of the d -wave component of the pairing gap. We did not find a theoretical justification for the first scenario, but we did find the argument for the second one.

Our analysis is similar to the one put forward by Fernandes and Millis [49], but we employ a somewhat different rationale and go beyond their analysis in the computation of the parameters in the free energy \mathcal{F} .

Consider for definiteness the hole d_{xy} pocket. Let us introduce a nematic order parameter $\Delta_n \cos 2\theta$. Because the d -wave gap component also scales as $\cos 2\theta$, \mathcal{F} should generally contain the term

$$\gamma \Delta_n (\Delta_s \Delta_d^* + \Delta_s^* \Delta_d). \quad (1)$$

Let us suppose that an s -wave order develops on its own at T_c , while nematic order and d -wave superconducting order do not develop in the absence of Δ_s . The free energy slightly below T_c is then

$$\begin{aligned} \mathcal{F} = & \alpha_s |\Delta_s|^2 + \beta_s |\Delta_s|^4 + \alpha_d |\Delta_d|^2 + \beta_d |\Delta_d|^4 + \alpha_n |\Delta_n|^2 \\ & + \beta_n |\Delta_n|^4 + 2\gamma \Delta_n |\Delta_s| |\Delta_d| \cos \phi + \dots, \end{aligned} \quad (2)$$

where ϕ is the relative phase between Δ_s and Δ_d and the dots stand for the terms which we will not need. By construction, $\alpha_s < 0$, while $\alpha_{d,n} > 0$ and $\beta_{s,d,n} > 0$. At $\gamma = 0$, $|\Delta_s|^2 = -\alpha_s / (2\beta_s)$, and $\Delta_d = \Delta_n = 0$. At a finite γ (of either sign), the minimization with respect to Δ_s , Δ_d , Δ_n , and ϕ yields

$$\begin{aligned} -\alpha_s |\Delta_s| + |\gamma| |\Delta_n| |\Delta_d| &= 2\beta_s |\Delta_s|^3, \\ -\alpha_s |\Delta_d| + |\gamma| |\Delta_n| |\Delta_s| &= 2\beta_d |\Delta_d|^3, \\ -\alpha_n |\Delta_n| + |\gamma| |\Delta_s| |\Delta_d| &= 2\beta_n |\Delta_n|^3. \end{aligned} \quad (3)$$

At small negative α_s the solution is an s -wave order ($\Delta_d = \Delta_n = 0$). However, as $|\alpha_s|$ increases, the system may simultaneously develop two other orders. This happens when

$$|\alpha_s|^{1/2} > \frac{(4\beta_s|\alpha_n\alpha_d|)^{1/2}}{\gamma} \quad \text{or} \quad \frac{|\alpha_s|}{|\alpha_n\alpha_d|^{1/2}} > \frac{4\beta_s|\Delta_s|}{\gamma}. \quad (4)$$

The inequality in Eq. (4) is definitely satisfied below some $T < T_c$ if the tendency towards nematic order and/or d -wave superconducting order is strong, i.e., the product $|\alpha_n\alpha_d|$ is small.

The coupling γ is graphically represented as a triangular diagram with Δ_n , Δ_s , and Δ_d in the vertices and three internal fermionic lines with momenta and frequencies (k, ω) , (k, ω) , and $(-k, -\omega)$. Evaluating the convolution of the three Green's functions with these momenta and frequencies and assuming parabolic dispersion for fermions near the d_{xy} hole pocket with $\epsilon_k = \mu - k^2/(2m)$, we obtain $|\gamma| = m/(16\pi\mu) = 1/(8\pi v_F^2)$. The coefficient β_s is obtained in a similar manner by evaluating the square diagram with Δ_s in the vertices and four fermionic lines, two with (k, ω) and two with $(-k, -\omega)$. Evaluating the convolution of the four fermionic Green's functions in the same way as in [50], we obtain $\beta_s = 7m\zeta(3)/(16\pi^3 T^2)$. Substituting the expressions for $|\gamma|$ and β_s into (4), we obtain the condition for s -wave-induced nematicity as

$$\frac{|\alpha_s|}{|\alpha_n\alpha_d|^{1/2}} > \frac{28\zeta(3)\mu|\Delta_s|}{\pi^2 T^2}. \quad (5)$$

For $T \sim T_c \sim \Delta_s$ it becomes $|\alpha_s| > A|\alpha_n\alpha_d|^{1/2}(\mu/T_c)$, where $A \geq 1$. For a system in which μ/T_c is large, the tendency towards nematic and/or d -wave instability near T_c must be strong; otherwise, the inequality on $|\alpha_s|$ would not be satisfied. In Fe-based materials, μ/T_c is not a very large number, and the probability that s -wave superconducting order will generate nematicity is much stronger.

Previous ARPES and scanning tunneling microscopy studies of the gap anisotropy [51–53] in LiFeAs were interpreted as evidence for a pure s -wave gap with $\cos 4\theta$ variation along the hole pockets. The breaking of the rotational symmetry was not detected in our earlier ARPES study [51] because of overall lower quality of the data, a smaller amount of data, and overlapping of the domains. The dominating contribution of the domains of one type in the present study could be a consequence of a small detwinning force due to, e.g., inhomogeneous hardening of the glue, cleavage-induced strains, or unequal thermal expansions. Regardless of the reason, although we were not able to detect significant distortions in the normal state, we cannot rule out a small C_4 symmetry breaking above T_c . Another explanation for the discrepancy with already published results could be poorer quality of earlier ARPES data. Finally, some earlier data were actually obtained by using a C_4 symmetrization procedure.

The observed spontaneous rotational symmetry breaking of the superconducting gap amplitude in LiFeAs is different from the symmetry breaking in d -wave or chiral- p -wave superconductors. In the latter only the phase acquires a new symmetry, and there is no change in the macroscopic state of the system under rotation; therefore, the rotational symmetry breaking can be detected only in interference experiments. In the present case the macroscopic state of the system does

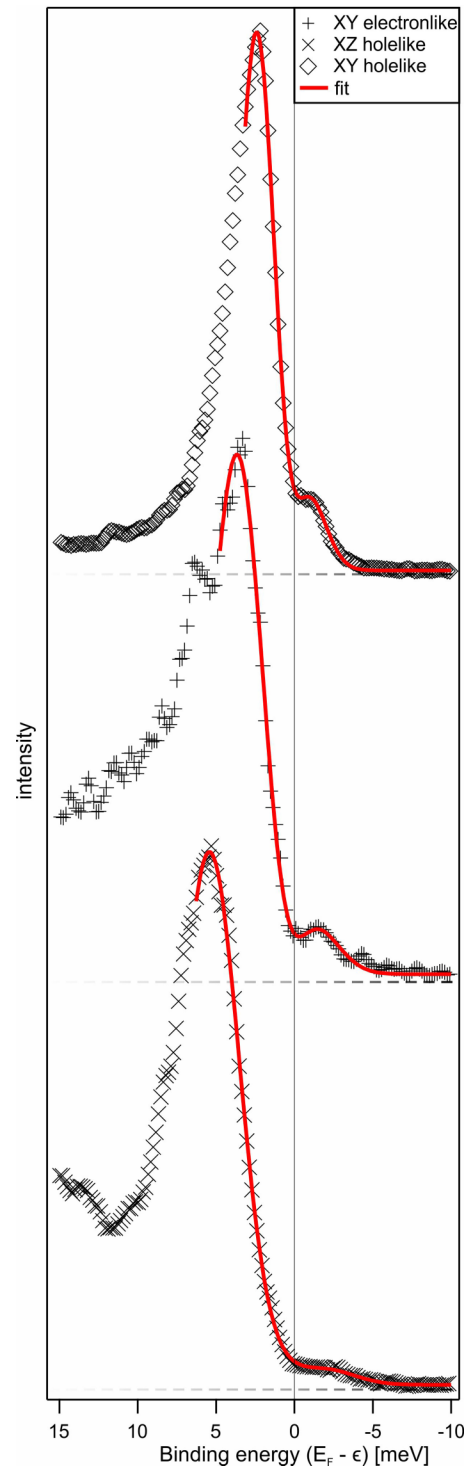


FIG. 5. Gap fitting.

change by the rotation, and thus, such symmetry breaking should be seen in bulk properties. Our data call for further, more detailed, and phase-sensitive experiments on LiFeAs and other IBSs.

ACKNOWLEDGMENTS

We are grateful to R. Fernandes, G. Behr, and C. Hess for fruitful discussions. We acknowledge the Diamond Light Source for time on Beamline I05 under proposals NT5008

and SI9689 and the BESSY II synchrotron. We are grateful to R. J. Cava, M. Ali, and Q. Gibson for providing us with YbMnBi₂ crystals, which we used for the device accuracy estimation. Y.S.K. and S.V.B. are supported by DFG Grants No. BO1912/6-1 and No. SPP1458. A.V.C. is supported by the Office of Basic Energy Sciences, U.S. Department of Energy, under Award No. DE-SC0014402. I.M. was supported by RSF-DFG Grant No. 19-43-04129.

APPENDIX A: DETAILS OF GAP EXTRACTION

EDCs in Fig. 1 exhibit very narrow coherent peaks. In the magenta EDC one can clearly distinguish the second coherent peak, which is located above the Fermi level. The distance between the peaks is 5.7 meV, but this distance is smaller than the real doubled gap size because the shape of the second peak is heavily distorted by the Fermi function. In order to extract the real gap size one should fit this EDC with a function which includes the influence of the Fermi function.

We fit EDCs with a function which consists of two peaks multiplied by the Fermi function and a background. Both peaks are Voigt profiles (convolution of a Lorentz profile and a Gaussian profile) with the same shape and size. They are located at equal distances from the Fermi level. The fitting function is as follows:

$$I(\epsilon) = I_0 + [I_1 + V(\epsilon - E_F - \Delta, A, W, S) + V(\epsilon - E_F + \Delta, A, W, S)]F(\epsilon, E_F, T),$$

where $F(\epsilon, E_F, T) = (1 + \exp(\frac{\epsilon - E_F}{kT}))^{-1}$ is the Fermi function and $V(x, A, W, S)$ is a Voigt profile. Here ϵ is the photoelectron kinetic energy; A , W , and S are numbers which represent the area, width, and ratio of the Lorentz and Gaussian components of the Voigt profile. E_F is the Fermi level position. Δ is the superconducting gap size. T is temperature, and k is the Boltzmann constant. The term $I_0 + I_1 F(\epsilon, E_F, T)$ represents a background. For the fitting I_0 , I_1 , E_F , Δ , A , W , S , and T are fit coefficients, and ϵ is an independent variable. During the fitting coefficient I_1 was held at a value which was estimated

TABLE I. Gap magnitude from EDC fitting.

Band	Gap size (meV)
XY holelike	2.30 ± 0.07
XY electronlike	3.57 ± 0.03
XZ holelike	5.41 ± 0.10

from part of the spectrum without bands. Changing this coefficient in a reasonable range makes only negligible changes in the fitting results. So holding I_1 constant should not cause inaccuracy in the gap size determination, and we can treat data in this way.

Figure 5 shows EDCs obtained from k_F for the XY holelike band (which forms a big pocket), the XY electronlike band (which forms an inner pocket), and the XZ holelike band (which forms a small pocket) from spectra in Fig. 1(b). The EDC for the XY holelike band was obtained from the 6 K spectrum, and two other EDCs were obtained from the 11 K spectrum. Results of fitting these EDCs with our function are given in Table I. The second coherent peak on the EDC obtained from the XZ holelike band is more distant from the Fermi level and, because of this, is more suppressed and appears as a shoulder. Nevertheless, in this case the gap can still be extracted from the fitting procedure.

There is one more peak at 6.5 meV on the EDC obtained from k_F for XY electron-like band. This peak originated from the XZ electronlike band (which forms an outer pocket).

In this way we determined the absolute values of the gap corresponding to the particular single EDCs from different parts of the Fermi surface. For the gap function determination we used the relative position of the leading edge of all EDCs along the given Fermi surface.

APPENDIX B: k_z DISPERSION

Figure 6 shows the k_z map, which allows us to determine the $h\nu$ corresponding to the G and Z points of the BZ. Z

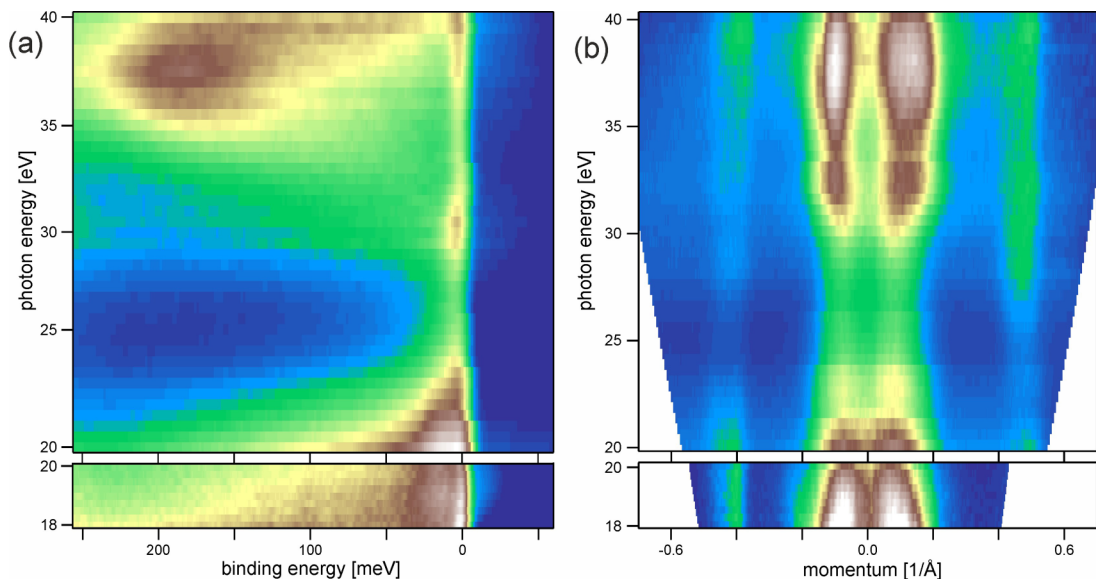


FIG. 6. k_z dispersion. (a) A set of EDCs which were obtained through the center of the holelike dispersion ($k_y = 0$) for different photon energies. (b) k_z map.

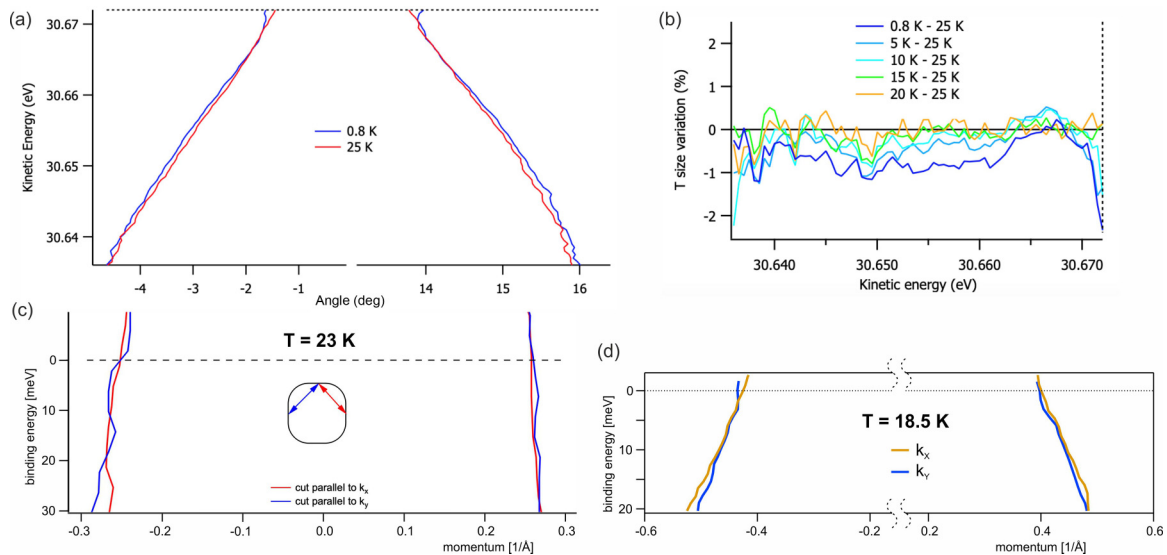


FIG. 7. (a) MDC dispersions of the d_{xy} bands forming the largest hole pocket obtained from spectra measured in the normal state (red curves) and superconducting state (blue curves). (b) Size variation caused by temperature. (c) Dispersions within the close vicinity of the Fermi level along two perpendicular cuts parallel to k_x (red curves) and k_y (blue curves) obtained from the data set measured at temperature above T_c . (d) Dispersions along the k_x (yellow curves) and k_y (blue curves) directions obtained from a different sample.

corresponds to ~ 37 eV, Γ corresponds to ~ 26 eV, and the next Z is at ~ 18 eV or a little bit lower.

APPENDIX C: DATA SUPPORTING THE SHIFTS OF THE DISPERSIONS WITH TEMPERATURE

The very unusual behavior reported by us in Fig. 2(f) can also be observed in yet another sample, and we show this result in Fig. 7(a). This time the shift can be clearly seen down to more than 30-meV binding energy.

We will quantify this shift with temperature further. We will also follow the temperature evolution in more detail, considering data taken at many more temperatures, not just comparing data above and below T_c .

To describe the temperature evolution of the shift we follow a procedure similar to those to determine the deformation coefficient. We obtain the value $2 \frac{L_{\text{normal}} - L_T}{L_{\text{normal}} + L_T}$, where L_T and L_{normal} are the distances between left and right dispersion at a particular temperature T and at 25 K, which corresponds to the normal state. Figure 7(b) shows the energy dependence of this value for different temperatures.

The obtained temperature behavior allows us to disentangle the effects of the superconducting gap opening

and nematicity-induced shifts. The orange curve (20–25 K) does not significantly deviate from zero in the full energy range, signaling the absence of any change in the dispersion as a function of temperature in the normal state. As the gap opens, we observe two effects: the dispersion starts to shift in the full energy range except near the gap value. This is because the dispersion develops the mentioned S shape. This local deviation is gone in the immediate vicinity to the Fermi level, and a clear change in k_F is detectable.

In Figs. 7(c) and 7(d) we present evidence for the absence of a detectable distortion of the Fermi surface in the normal state. In Fig. 7(c) the dispersions corresponding to the cuts parallel to the diagonals of the FS (see inset) from the same cleave as other data from Fig. 2 are shown. Figure 7(d) shows the shape of d_{xy} dispersions along the k_x and k_y directions [equivalent to Fig. 2(d)] at a temperature above T_c . These dispersions are extracted from two data sets measured before and after the rotation of the sample by 90° (the sample is different from the one from which the results presented in the main text were obtained). Neither plot shows any considerable deformation.

- [1] J. Tranquada, B. Sternlieb, J. Axe, Y. Nakamura, and S. Uchida, *Nature (London)* **375**, 561 (1995).
- [2] W. Li, Y. Zhang, P. Deng, Z. Xu, S.-K. Mo, M. Yi, H. Ding, M. Hashimoto, R. Moore, D.-H. Lu *et al.*, *Nat. Phys.* **13**, 957 (2017).
- [3] R. Borzi, S. Grigera, J. Farrell, R. Perry, S. Lister, S. Lee, D. Tennant, Y. Maeno, and A. Mackenzie, *Science* **315**, 214 (2007).
- [4] J.-H. Chu, J. G. Analytis, K. De Greve, P. L. McMahon, Z. Islam, Y. Yamamoto, and I. R. Fisher, *Science* **329**, 824 (2010).
- [5] A. V. Chubukov and P. J. Hirschfeld, *Phys. Today* **68**(6), 46 (2015).
- [6] R. Fernandes, A. Chubukov, and J. Schmalian, *Nat. Phys.* **10**, 97 (2014).
- [7] S. Baek, D. Efremov, J. Ok, J. Kim, J. Van Den Brink, and B. Büchner, *Nat. Mater.* **14**, 210 (2015).
- [8] R. Khasanov, M. Bendele, K. Conder, H. Keller, E. Pomjakushina, and V. Pomjakushin, *New J. Phys.* **12**, 073024 (2010).
- [9] M. Rotter, M. Tegel, D. Johrendt, I. Schellenberg, W. Hermes, and R. Pöttgen, *Phys. Rev. B* **78**, 020503(R) (2008).

- [10] Q. Huang, Y. Qiu, W. Bao, M. A. Green, J. W. Lynn, Y. C. Gasparovic, T. Wu, G. Wu, and X. H. Chen, *Phys. Rev. Lett.* **101**, 257003 (2008).
- [11] A. I. Goldman, D. N. Argyriou, B. Ouladdiaf, T. Chatterji, A. Kreyssig, S. Nandi, N. Ni, S. L. Bud'Ko, P. C. Canfield, and R. J. McQueeney, *Phys. Rev. B* **78**, 100506(R) (2008).
- [12] A. Fedorov, A. Yaresko, T. K. Kim, Y. Kushnirenko, E. Haubold, T. Wolf, M. Hoesch, A. Grueneis, B. Büchner, and S. Borisenko, *Sci. Rep.* **6**, 36834 (2016).
- [13] M. D. Watson, T. K. Kim, L. C. Rhodes, M. Eschrig, M. Hoesch, A. A. Haghighirad, and A. I. Coldea, *Phys. Rev. B* **94**, 201107(R) (2016).
- [14] V. K. Thorsmølle, M. Khodas, Z. P. Yin, C. Zhang, S. V. Carr, P. Dai, and G. Blumberg, *Phys. Rev. B* **93**, 054515 (2016).
- [15] P. Massat, D. Farina, I. Paul, S. Karlsson, P. Strobel, P. Toulemonde, M.-A. Méasson, M. Cazayous, A. Sacuto, S. Kasahara *et al.*, *Proc. Natl. Acad. Sci. USA* **113**, 9177 (2016).
- [16] Y. Yamakawa, S. Onari, and H. Kontani, *Phys. Rev. X* **6**, 021032 (2016).
- [17] L. Benfatto, B. Valenzuela, and L. Fanfarillo, *npj Quantum Mater.* **3**, 56 (2018).
- [18] L. Fanfarillo, G. Giovannetti, M. Capone, and E. Bascones, *Phys. Rev. B* **95**, 144511 (2017).
- [19] M. Chinotti, A. Pal, L. Degiorgi, A. E. Böhmer, and P. C. Canfield, *Phys. Rev. B* **96**, 121112(R) (2017).
- [20] M. Toyoda, Y. Kobayashi, and M. Itoh, *Phys. Rev. B* **97**, 094515 (2018).
- [21] S. Lederer, Y. Schattner, E. Berg, and S. A. Kivelson, *Phys. Rev. Lett.* **114**, 097001 (2015).
- [22] A. Klein, S. Lederer, D. Chowdhury, E. Berg, and A. Chubukov, *Phys. Rev. B* **98**, 041101(R) (2018).
- [23] K. Matsuura, Y. Mizukami, Y. Arai, Y. Sugimura, N. Maejima, A. Machida, T. Watanuki, T. Fukuda, T. Yajima, Z. Hiroi *et al.*, *Nat. Commun.* **8**, 1143 (2017).
- [24] Y. S. Hor, A. J. Williams, J. G. Checkelsky, P. Roushan, J. Seo, Q. Xu, H. W. Zandbergen, A. Yazdani, N. P. Ong, and R. J. Cava, *Phys. Rev. Lett.* **104**, 057001 (2010).
- [25] S. Yonezawa, K. Tajiri, S. Nakata, Y. Nagai, Z. Wang, K. Segawa, Y. Ando, and Y. Maeno, *Nat. Phys.* **13**, 123 (2017).
- [26] L. Fu and E. Berg, *Phys. Rev. Lett.* **105**, 097001 (2010).
- [27] M. Hecker and J. Schmalian, *npj Quantum Mater.* **3**, 1 (2018).
- [28] C.-w. Cho, J. Shen, J. Lyu, O. Atanov, Q. Chen, S. H. Lee, Y. S. Hor, D. J. Gawryluk, E. Pomjakushina, M. Bartkowiak *et al.*, *Nat. Commun.* **11**, 3056 (2020).
- [29] J. W. F. Venderbos and R. M. Fernandes, *Phys. Rev. B* **98**, 245103 (2018).
- [30] J. F. Dodaro, S. A. Kivelson, Y. Schattner, X.-Q. Sun, and C. Wang, *Phys. Rev. B* **98**, 075154 (2018).
- [31] V. Kozii, H. Isobe, J. W. F. Venderbos, and L. Fu, *Phys. Rev. B* **99**, 144507 (2019).
- [32] M. S. Scheurer and R. Samajdar, *Phys. Rev. Research* **2**, 033062 (2020).
- [33] D. V. Chichinadze, L. Classen, and A. V. Chubukov, *Phys. Rev. B* **101**, 224513 (2020).
- [34] Y. Cao, *Bull. Am. Phys. Soc.* **65**, 1 (2020).
- [35] S. V. Borisenko, V. B. Zabolotnyy, D. V. Evtushinsky, T. K. Kim, I. V. Morozov, A. N. Yaresko, A. A. Kordyuk, G. Behr, A. Vasiliev, R. Follath, and B. Büchner, *Phys. Rev. Lett.* **105**, 067002 (2010).
- [36] C. M. Yim, C. Trainer, R. Aluru, S. Chi, W. N. Hardy, R. Liang, D. Bonn, and P. Wahl, *Nat. Commun.* **9**, 2602 (2018).
- [37] I. Morozov, A. Boltalin, O. Volkova, A. Vasiliev, O. Kataeva, U. Stockert, M. Abdel-Hafiez, D. Bombor, A. Bachmann, L. Harnagea *et al.*, *Cryst. Growth Des.* **10**, 4428 (2010).
- [38] M. Hoesch, T. Kim, P. Dudin, H. Wang, S. Scott, P. Harris, S. Patel, M. Matthews, D. Hawkins, S. Alcock *et al.*, *Rev. Sci. Instrum.* **88**, 013106 (2017).
- [39] See Supplemental Material at <http://link.aps.org/supplemental/10.1103/PhysRevB.102.184502> for data which shows intermediate steps of the superconducting gap anisotropy and the FS deformation extraction and data which demonstrates the calibration precision of the ARPES setup.
- [40] S. V. Borisenko, D. V. Evtushinsky, Z.-H. Liu, I. Morozov, R. Kappenberger, S. Wurmehl, B. Büchner, A. N. Yaresko, T. K. Kim, M. Hoesch, T. Wolf, and N. D. Zhigadlo, *Nat. Phys.* **12**, 311 (2016).
- [41] R. P. Day, G. Levy, M. Michiardi, B. Zwartsenberg, M. Zonno, F. Ji, E. Razzoli, F. Boschini, S. Chi, R. Liang, P. K. Das, I. Vobornik, J. Fujii, W. N. Hardy, D. A. Bonn, I. S. Elfimov, and A. Damascelli, *Phys. Rev. Lett.* **121**, 076401 (2018).
- [42] M. R. Norman, M. Eschrig, A. Kaminski, and J. C. Campuzano, *Phys. Rev. B* **64**, 184508 (2001).
- [43] A. V. Chubukov and M. R. Norman, *Phys. Rev. B* **70**, 174505 (2004).
- [44] A. A. Kordyuk, V. B. Zabolotnyy, D. V. Evtushinsky, T. K. Kim, I. V. Morozov, M. L. Kulić, R. Follath, G. Behr, B. Büchner, and S. V. Borisenko, *Phys. Rev. B* **83**, 134513 (2011).
- [45] F. Ahn, I. Eremin, J. Knolle, V. B. Zabolotnyy, S. V. Borisenko, B. Büchner, and A. V. Chubukov, *Phys. Rev. B* **89**, 144513 (2014).
- [46] Z. Yin, K. Haule, and G. Kotliar, *Nat. Phys.* **10**, 845 (2014).
- [47] T. Saito, S. Onari, Y. Yamakawa, H. Kontani, S. V. Borisenko, and V. B. Zabolotnyy, *Phys. Rev. B* **90**, 035104 (2014).
- [48] Y. Wang, A. Kreisel, V. B. Zabolotnyy, S. V. Borisenko, B. Büchner, T. A. Maier, P. J. Hirschfeld, and D. J. Scalapino, *Phys. Rev. B* **88**, 174516 (2013).
- [49] R. M. Fernandes and A. J. Millis, *Phys. Rev. Lett.* **111**, 127001 (2013).
- [50] R. M. Fernandes, A. V. Chubukov, J. Knolle, I. Eremin, and J. Schmalian, *Phys. Rev. B* **85**, 024534 (2012).
- [51] S. V. Borisenko, V. B. Zabolotnyy, A. A. Kordyuk, D. V. Evtushinsky, T. K. Kim, I. V. Morozov, R. Follath, and B. Büchner, *Symmetry* **4**, 251 (2012).
- [52] M. Allan, A. Rost, A. Mackenzie, Y. Xie, J. Davis, K. Kihou, C. Lee, A. Iyo, H. Eisaki, and T.-M. Chuang, *Science* **336**, 563 (2012).
- [53] K. Umezawa, Y. Li, H. Miao, K. Nakayama, Z.-H. Liu, P. Richard, T. Sato, J. B. He, D.-M. Wang, G. F. Chen, H. Ding, T. Takahashi, and S.-C. Wang, *Phys. Rev. Lett.* **108**, 037002 (2012).